Spectrochimica Acta Part A: Molecular and Biomolecular Spectroscopy 262 (2021) 120087

Contents lists available at ScienceDirect

Spectrochimica Acta Part A: Molecular and Biomolecular Spectroscopy

journal homepage: www.elsevier.com/locate/saa

Ratiometric fluorescent sensor based on MoS_2 QDs and AuNCs for determination and bioimaging of alkaline phosphatase

Yibing Liu [a], Yu Zhang [c], Wei Zhang [a], Xinghua Wang [a], Ying Sun [a], Yibing Huang [c], Pinyi Ma [a], Jun Ding [b,*], Daqian Song [a,*]

[a] College of Chemistry, Jilin Province Research Center for Engineering and Technology of Spectral Analytical Instruments, Jilin University, Qianjin Street 2699, Changchun 130012, China
[b] China-Japan Union Hospital of Jilin University, Sendai Street 126, Changchun 130033, China
[c] College of Life Sciences, Jilin University, Qianjin Street 2699, Changchun 130012, China

HIGHLIGHTS

- A ratiometric fluorescent sensor was developed for ALP detection and imaging.
- Ratiometric detection endowed the sensor with high sensitivity and accuracy.
- The sensor was employed in lysosome localization and imaging of intracellular ALP.

GRAPHICAL ABSTRACT

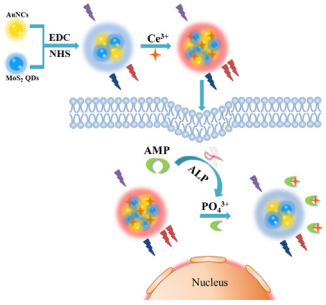

ARTICLE INFO

Article history:
Received 10 May 2021
Received in revised form 8 June 2021
Accepted 15 June 2021
Available online 17 June 2021

Keywords:
Alkaline phosphatase
Ratiometric fluorescent sensor
Gold nanoclusters
Quantum dots
Cell imaging

ABSTRACT

Herein, a ratiometric fluorescent sensor based on MoS_2 quantum dots (QDs) and glutathione-capped gold nanoclusters (AuNCs) was developed for determination and imaging of alkaline phosphatase (ALP). The sensor was developed by covalently linking QDs with AuNCs to form stable MoS_2@AuNCs nanohybrids that exhibited the blue fluorescence of MoS_2 QDs and the red fluorescence of AuNCs. In the presence of Ce^{3+}, the fluorescence intensity of AuNCs was increased due to the aggregation-induced emission enhancement (AIEE), while that of MoS_2 QDs remained unchanged, thus could be used as a reference signal. After adenosine 5′-monophosphate (AMP) and ALP were introduced into the system, AMP was hydrolyzed to adenosine and phosphate ions (PO_4^{3-}). Owing to higher affinity between Ce^{3+} and PO_4^{3-}, the AIEE effect was inhibited, in turn resulting in the decrease of AuNCs fluorescence. The developed ratiometric fluorescent sensor had a linear response to ALP concentration ranging from 0.5 to 50 U L^{-1} with a detection limit (LOD) of 0.08 U L^{-1}. Moreover, the sensor had low cytotoxicity and was successfully employed in lysosome localization and bioimaging of intracellular ALP in living cells.

© 2021 Elsevier B.V. All rights reserved.

1. Introduction

Alkaline phosphatase (ALP), a membrane-binding enzyme, is widely distributed in biological tissues, such as liver, kidney, bone, intestine and placenta [1–3]. ALP can hydrolyze phosphate groups in small molecules, proteins and nucleic acids [4,5]. It also plays vital role in signal transduction and in the regulation of intracellular processes, including cell growth and apoptosis [6,7]. An abnormal serum ALP level is found to closely linked to many diseases, such as bone disease, liver dysfunction, prostate cancer and other diseases [8,9]. In addition, ALP, as a secretory protein, can also reflect the biological activity of cells [10,11]. Real-time monitoring of intercellular ALP allows the distinguishing between normal and abnormal cell behaviors [12]. Therefore, developing a sensitive, reliable and convenient method for determination and bioimaging

* Corresponding authors.
E-mail addresses: dingjun@jlu.edu.cn (J. Ding), songdq@jlu.edu.cn (D. Song).

https://doi.org/10.1016/j.saa.2021.120087
1386-1425/© 2021 Elsevier B.V. All rights reserved.

of ALP is of great significance. Up to now, numerous methods have been employed for ALP detection, including colorimetry [13,14], electrochemistry [15,16], surface-enhanced Raman scattering [17,18] and fluorometry [19,20]. Among these methods, the fluorescence method is attractive due to its many advantages, including simple operation, high sensitivity and ability in real-time monitoring of living cells [21]. Furthermore, dual-signal readout analysis method has attracted much attention because of its ability to reduce interferences from complex matrixes and its high sensitivity [22]. It is necessary to develop a new ratiometric fluorescent method with low toxicity using simple preparation processes for detection and bioimaging of ALP.

The unique optical properties of MoS_2 quantum dots (QDs) allow them to become the ideal candidates for optical sensors [23]. Moreover, due to their good cell permeability, low toxicity and excellent biocompatibility, MoS_2 QDs are widely used in living cell imaging [24]. Gold nanoclusters (AuNCs), as a type of fascinating luminescent nanomaterials, have long luminescence lifetime, good photostability and aggregation-induced emission enhancement (AIEE) characteristic [25]. AuNCs with AIEE characteristic have been successfully applied in optical sensors and cell imaging [26]. However, most of the existing methods depend only on the fluorescence intensity changes of individual components in the system. In contrast to single channel fluorescence assays, ratiometric fluorescent techniques have built-in interference correction ability [27]. Thus, constructing a ratiometric sensor by combining QDs with AuNCs can be of great significance.

Herein, we constructed a ratiometric fluorescent sensor by covalently linking MoS_2 QDs with AuNCs through a condensation reaction. The fluorescence of MoS_2 QDs was nearly unchanged with time, thus could act as a reference signal. In the presence of Ce^{3+}, the fluorescence intensity of AuNCs increased due to their aggregation-induced emission enhancement characteristic [28]. After the addition of adenosine 5′-monophosphate (AMP; a substrate of ALP) and ALP, AMP was hydrolyzed to adenosine and phosphate ions (PO_4^{3-}). Owing to the high affinity between Ce^{3+} and PO_4^{3-}, the Ce^{3+}-induced AIEE process was inhibited, causing the fluorescence intensity of AuNCs to decrease. Based on the above mechanisms, the developed ratiometric MoS_2@AuNCs nanohybrids sensor was able to detect ALP activity. Furthermore, as the covalent link can ensure that the uptake of the two nanomaterials by the cells is constant, thus, the sensor can be used for quantitative detection of intracellular substances, as well as for intracellular localization. The sensor was successfully applied in the bioimaging of intracellular ALP and lysosome co-localization.

2. Experimental section

2.1. Synthesis of MoS_2 QDs, AuNCs and MoS_2@AuNCs

MoS_2 QDs were synthesized by a one-pot hydrothermal method according to a previous report [29]. Firstly, 0.5 g of $Na_2MoO_4{\cdot}2H_2O$ was dissolved in 6.25 mL of water and then ultrasonicated for 5 min. After 1.25 g of cysteamine hydrochloride and 12.5 mL of water were added, the mixture was further sonicated for another 10 min. After that, the pH of the mixture was adjusted to 6.0 with 0.1 M HCl. The mixture was then transferred to a Teflon-lined stainless steel autoclave (30 mL), in which the reaction was allowed to take place for 36 h at 200 °C. After cooling down to room temperature, the mixture was centrifuged at 11000 rpm for 10 min, and the supernatant was collected and then filtered through a 0.22 μm microporous membrane. The obtained QDs were stored at 4 °C for future use.

AuNCs were prepared based on a previously reported method [30]. Six milliliters of freshly prepared glutathione (10 mM) was mixed with 0.4 mL of $HAuCl_4$ (100 mM) and 13.6 mL of ultrapure water, and the mixture was vigorously stirred at 25 °C for 5 min. The solution was further stirred at 450 rpm at 70 °C for 24 h until its color turned pale yellow. The obtained AuNCs were stored at 4 °C until subsequent use.

To prepare MoS_2@AuNCs, 5 mg of EDC and 5 mg of NHS were reacted with 1 mL of AuNCs for 30 min to activate the carboxyl groups of AuNCs. After 1 mL of MoS_2 QDs was added, the mixture was stirred for 2 h and then incubated at 4 °C overnight. The product was purified by dialysis against deionized water (MWCO of 1000) for 24 h and then dried under vacuum.

2.2. Fluorometric determination of ALP

In ALP determination, 50 μL of Ce^{3+} (1 mM), 10 μL of Mg^{2+} (0.1 μM), 10 μL of Ca^{2+} (0.05 μM), 100 μL of AMP (5 mM), and 100 μL of ALP at different concentrations were mixed in 710 μL of Tris-HCl buffer (10 mM, pH 8). The mixture was allowed to react for 40 min at 37 °C and added with 20 μL of MoS_2@AuNCs (5 mg mL^{-1}) thereafter. The fluorescence spectrum was recorded from 400 nm to 750 nm at an excitation wavelength of 350 nm.

2.3. Cytotoxicity assay and cell imaging

The cytotoxicity of MoS_2@AuNCs was examined by MTT assay. A549 cells (provided by the Life Sciences College of Jilin University) seeded in a 96-well plate were treated with different concentrations of MoS_2@AuNCs (0.025–1 mg mL^{-1}) for 24 h at 37 °C. Subsequently, 20 μL of 5 mg mL^{-1} MTT solution was added into each well and was removed after 4-h incubation. After adding 150 μL of dimethyl sulfoxide (DMSO) to each well, the plates were shaken for 5 min. The plate was subjected to measurement of an absorbance at 490 nm using a microplate reader.

For cell imaging, A549 cells were seeded in Dulbecco's Modified Eagle Medium (DMEM) supplemented with 10% fetal bovine serum (FBS) at 37 °C under 5% CO_2 atmosphere for 24 h. After that, the cells were incubated with 1 mg mL^{-1} MoS_2@AuNCs for 4 h. Thereafter, the cells were treated with Ce^{3+} (1 mM) for 5 min, or with Ce^{3+} (1 mM) and AMP (20 mM) for 15 min and 40 min. For co-localization experiments, the cells were incubated with 1 mg mL^{-1} MoS_2@AuNCs for 4 h, followed by LysoTracker Green for another 20 min. The cells were subjected to imaging by a laser scanning confocal microscope.

3. Results and discussion

3.1. Characterization of MoS_2 QDs, AuNCs and MoS_2@AuNCs

According to the transmission electron microscope (TEM) images, MoS_2 QDs had a uniform spherical shape with an average particle size of about 4.1 nm (Fig. 1A), and AuNCs had an average size of 2.5 nm and were evenly distributed (Fig. 1B). The TEM image of MoS_2@AuNCs nanohybrids (Fig. 1C) showed that they had conjugated structure. Based on preparation procedures, the conjugated structure should be attributed to the coupling between MoS_2 QDs and AuNCs. To further prove the coupling in MoS_2@AuNCs, Fourier transform infrared spectrum (FT-IR spectra) of MoS_2 QDs, AuNCs, and MoS_2@AuNCs nanohybrids were recorded. Fig. 1D displays the FT-IR spectra of MoS_2 QDs, AuNCs and MoS_2@AuNCs. The absorption peaks of MoS_2 QDs at 3134 and 3039 cm^{-1} were due to the stretching vibration of N-H. The peak at 1651 cm^{-1} was corresponded to the strong N-H deformation, whereas that at 1402 cm^{-1} was due to the vibration of C-N bond [31]. The characteristic peaks of the S-H stretching band of cysteamine (around 2223 cm^{-1}) disappeared [29]. These results demonstrated the suc-

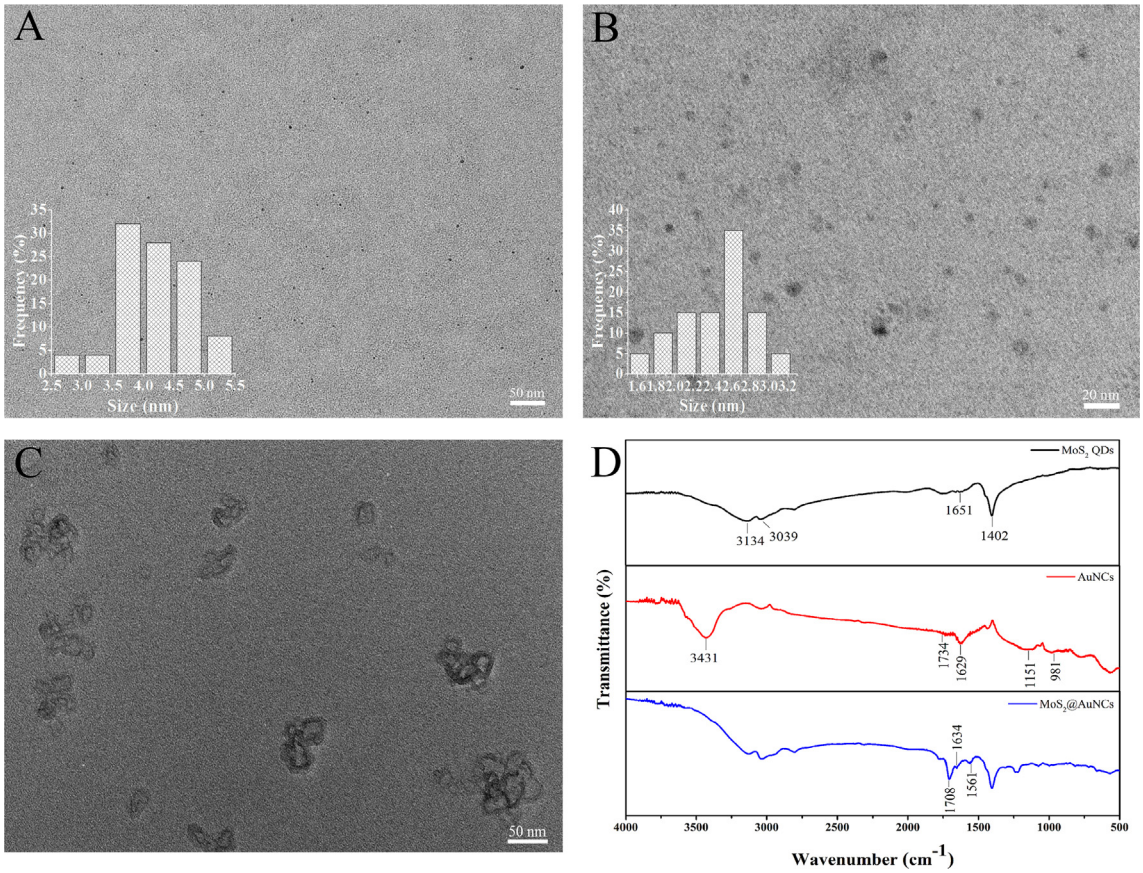

Fig. 1. TEM image and size distribution histogram (inset) of (A) MoS_2 QDs and (B) AuNCs. (C) TEM image of MoS_2@AuNCs. (D) FT-IR spectra of MoS_2 QDs, AuNCs and MoS_2@AuNCs.

cessful modification of cysteamine and linkage of amino groups on the surface of QDs. After AuNCs were formed, the band of sulfhydryl group in pure glutathione at 2526 cm^{-1} disappeared, which indicated that the S-Au bond had been formed [32]. AuNCs also exhibited the peak corresponding to the stretching vibrations of O—H and N—H at 3431 cm^{-1}, and peak corresponding to the stretching vibrations of C═O in carboxyl groups at 1629 cm^{-1} [33]. In addition, the peak located at 1151 cm^{-1} was ascribed to the vibrations of C—O—C [34]. For MoS_2@AuNCs nanohybrids, the absorption peaks at 1634 and 1708 cm^{-1} were assigned to the C═O stretching vibration of acrylamide [35], and the peak at 1561 cm^{-1} was assigned to the amide groups (–CONH) [36]. These results further confirm that amide bonds were successfully formed, and QDs and AuNCs were successfully combined. Fig. S1 shows the fluorescence spectra of MoS_2 QDs, AuNCs, and MoS_2@AuNCs. MoS_2 QDs exhibited a blue emission peak at 433 nm, and AuNCs exhibited a red emission peak at 637 nm. After the two materials were coupled, the resultant ratiometric MoS_2@AuNCs exhibited two well-resolved emission peaks at both 475 nm and 675 nm. Compared to that of QDs and AuNCs, the fluorescence peaks of the nanocomposite MoS_2@AuNCs were red-shifted, indicating that the obtained nanohybrid fluorescent spectrum was not the result of the physical mixing between QDs and AuNCs. These results also confirm the successful coupling between QDs and AuNCs.

3.2. Sensing mechanism of the developed ratiometric sensor

The attractive aggregation-induced emission enhancement (AIEE) characteristic of thiolated AuNCs allows the sensor to have higher brightness. According to a previous report, Ce^{3+} can trigger the aggregation of glutathione-capped AuNCs and enhance the fluorescence intensity [28]. Owing to the strong affinity between Ce^{3+} and carboxylate groups of the glutathione ligands, Ce^{3+} can drive the assembly of AuNCs and induce their AIEE characteristic. As shown in the TEM image of MoS_2@AuNCs with the addition of Ce^{3+} (Fig. S2), significant aggregation can be observed. The resonance light scattering (RLS) spectroscopy of MoS_2@AuNCs with different concentrations of Ce^{3+} was shown in Fig. S3. RLS technique is proved an effective method to investigate aggregate systems, aggregation will lead to enhanced RLS signal [37]. With the increase of Ce^{3+} concentration, the RLS intensity increased gradually, this also demonstrated the aggregation of MoS_2@AuNCs. The above results proved the AIEE process between MoS_2@AuNCs and Ce^{3+}. Based on this principle, we covalently linked amino-modified MoS_2 QDs and glutathione-capped AuNCs to construct a ratiometric fluorescent sensor MoS_2@AuNCs (Scheme 1). In the presence of Ce^{3+}, the fluorescence emission of AuNCs was significantly enhanced, whereas that of MoS_2 QDs (an internal standard) remained nearly unchanged. AMP is a natural ALP substrate that can be hydrolyzed to adenosine and phosphate ions (PO_4^{3-}). After incubating ALP with AMP, Ce^{3+} can be desorbed from the surface of MoS_2@AuNCs because the affinity between Ce^{3+} and PO_4^{3-} is higher than that between Ce^{3+} and carboxylic group [38,39]. Thus, the fluorescence intensity of AuNCs decreased with increasing ALP concentration, while that of MoS_2 QDs was constant and could serve as a reference signal. Based on the results and analysis mentioned above, a ratio fluorescence assay for determining ALP activity was developed.

3.3. Optimization in ALP detection

To achieve a ratiometric sensor with the best performance, the ALP detection conditions were optimized. In the presence of Ce^{3+},

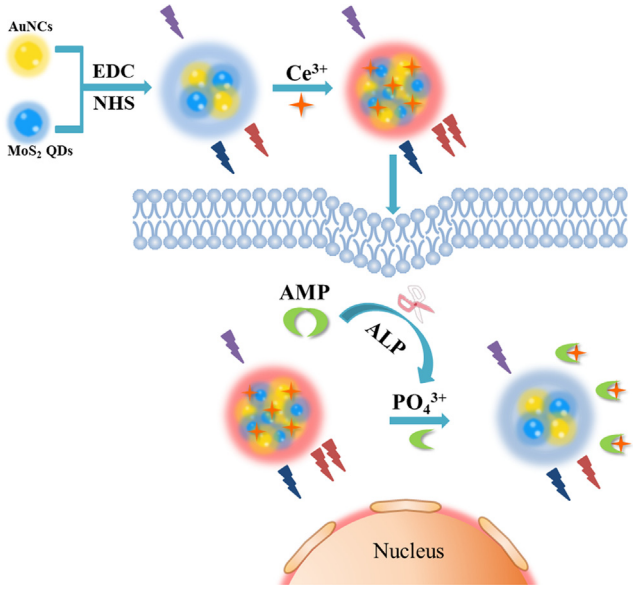

Scheme 1. Schematic illustration showing the ALP detection mechanism of MoS_2@AuNCs.

the fluorescence intensity at 675 nm of MoS_2@AuNCs increased gradually, while that at 475 nm (the reference signal) was constant (Fig. 2B). When the concentration of Ce^{3+} reached 50 μM, the fluorescence intensity ratio (F_{675}/F_{457} ratio) reached its maximum value; thus, 50 μM Ce^{3+} was used in the following experiment. Fig. S4 shows the change of F_{675}/F_{457} ratio with AMP concentration. At the AMP concentration of 0.5 mM, the F_{675}/F_{457} ratio was constant; therefore, 0.5 mM AMP was sufficient to meet the experimental requirement. The performance of the sensor at different pH was further examined (Fig. S5), and the results showed that the sensor had the best performance at pH 8.0. As shown in Fig. S6, after incubating for 40 min, the F_{675}/F_{457} ratio reached the plateau, indicating that the optimal reaction time was 40 min.

3.4. Ratiometric determination of ALP

The feasibility in detecting ALP of the ratiometric fluorescent sensor was investigated. As shown in Fig. 2A, upon the addition of Ce^{3+}, the fluorescence intensity at 675 nm increased, while that at 475 nm remained nearly unchanged. After the addition of AMP, the fluorescence of the ratiometric sensor was not obviously changed. However, when ALP was added into the solution, the fluorescence intensity at 675 nm decreased, and that at 475 nm was

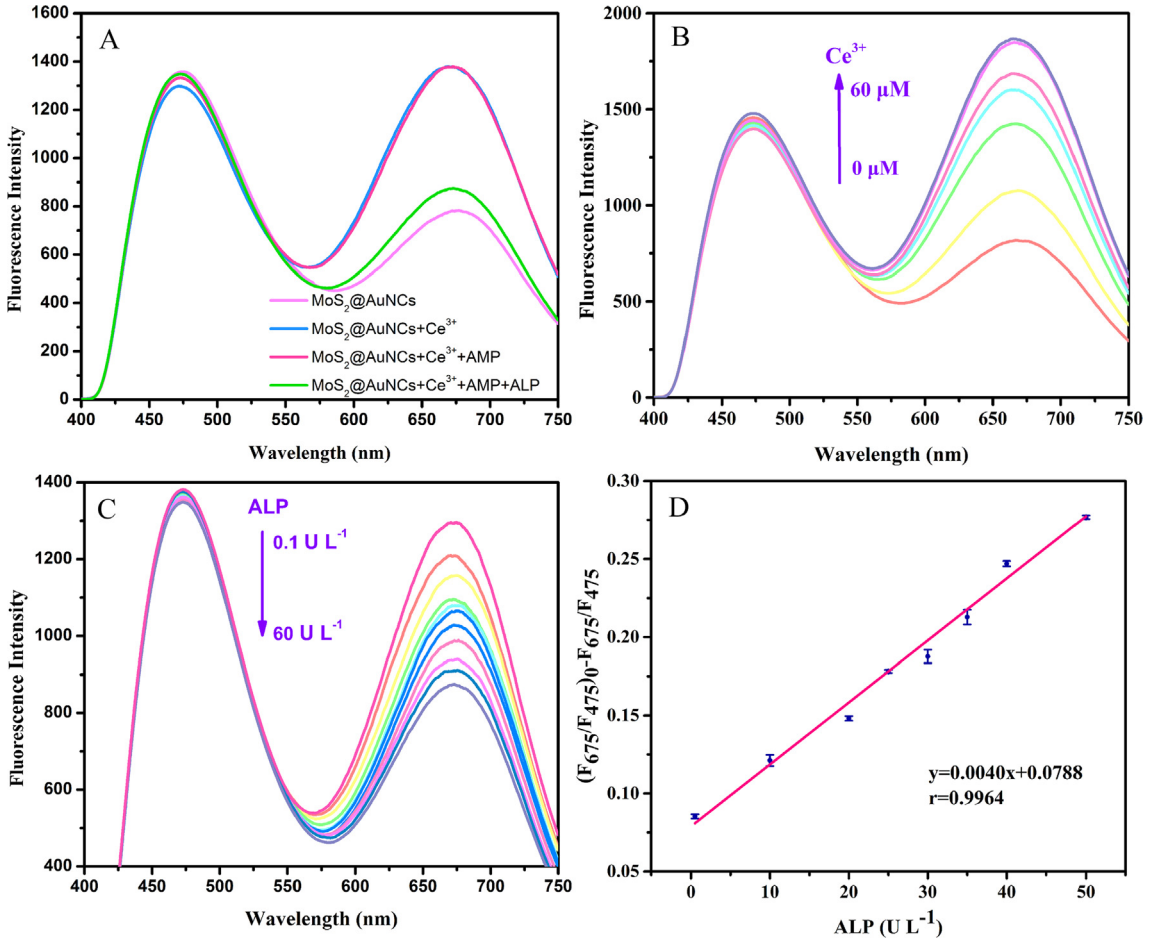

Fig. 2. (A) Fluorescence spectra of MoS_2@AuNCs, MoS_2@AuNCs + Ce^{3+}, MoS_2@AuNCs + Ce^{3+} + AMP, and MoS_2@AuNCs + Ce^{3+} + AMP + ALP (incubated at 37 °C for 40 min). Concentrations: MoS_2@AuNCs, 0.1 mg mL^{-1}; Ce^{3+}, 50 μM; AMP, 0.5 mM; and ALP, 50 U L^{-1}. (B) Fluorescence spectra of MoS_2@AuNCs in the presence of Ce^{3+} at different concentrations. (C) Fluorescence spectra of MoS_2@AuNCs in the presence of ALP at different concentrations. (D) Linear relationship between $(F_{675}/F_{475})_0$-F_{675}/F_{475} and ALP concentration. $(F_{675}/F_{475})_0$ and F_{675}/F_{475} are the fluorescence intensity ratio before and after the addition of ALP, respectively.

unchanged, thus could act as a reference signal and a built-in interference correction. The performance in ALP detection of the ratiometric sensing system was assessed under the optimal conditions. Fig. 2C shows the change of fluorescence intensity of MoS_2@AuNCs with ALP concentration ranging from 0.1 to 60 U L^{-1}: while the fluorescence intensity at 675 nm decreased, that at 475 nm was almost unchanged. As illustrated in Fig. 2D, the linear detection range of the ratiometric sensor was 0.5–50 U L^{-1} with the regression equation: $(F_{675}/F_{475})_0$ - F_{675}/F_{475} = 0.004 [ALP] + 0.0788 (r = 0.9964), where $(F_{675}/F_{475})_0$ and F_{675}/F_{475} are the ratio of the fluorescence intensity at 675 nm and that at 475 nm without and with the addition of ALP, respectively. The detection limit (LOD) of the sensor was calculated to be 0.08 U L^{-1}. The comparison between the performance in ALP determination of the present ratiometric fluorescent sensor and that of other methods was listed in Table S1.

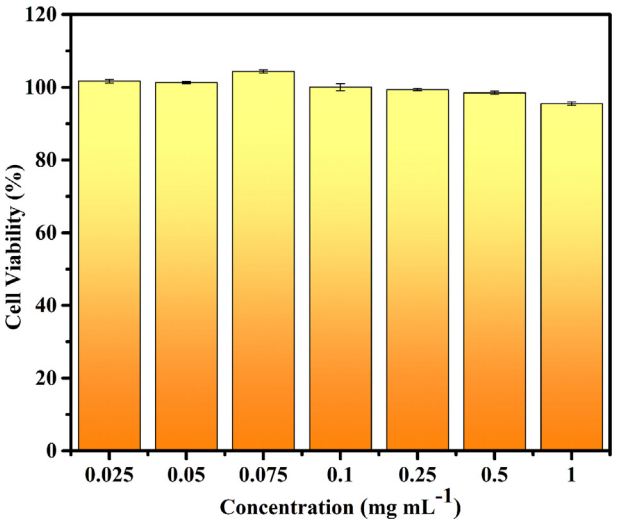

Fig. 3. Viability of A549 cells incubated with MoS_2@AuNCs.

3.5. Selectivity and determination of ALP in human serum samples

To determine the selectivity towards ALP of the developed ratiometric sensor, the influence of some interferences, including inorganic ions (Na^+, K^+, and Ca^{2+}), small biomolecules (cysteine (Cys), glutathione (GSH), and glucose (Glu)), proteins and enzymes (bovine serum albumin (BSA), IgG, horseradish peroxidase (HRP), glucose oxidase (GOx), tyrosinase (TYR), trypsin (Tryp), and acid phosphatase (ACP)) on the fluorescence of MoS_2@AuNCs was investigated. As displayed in Fig. S7, other than ALP, these interferences had no obvious effects on the fluorescence of MoS_2@AuNCs. The above results indicate that the sensor had high selectivity towards ALP.

To verify the applicability of the present ratiometric sensor in complex systems, ALP activity in human serum samples diluted by 20 folds was determined. The results summarized in Table S2 showed that the average recoveries of ALP in spiked serum samples

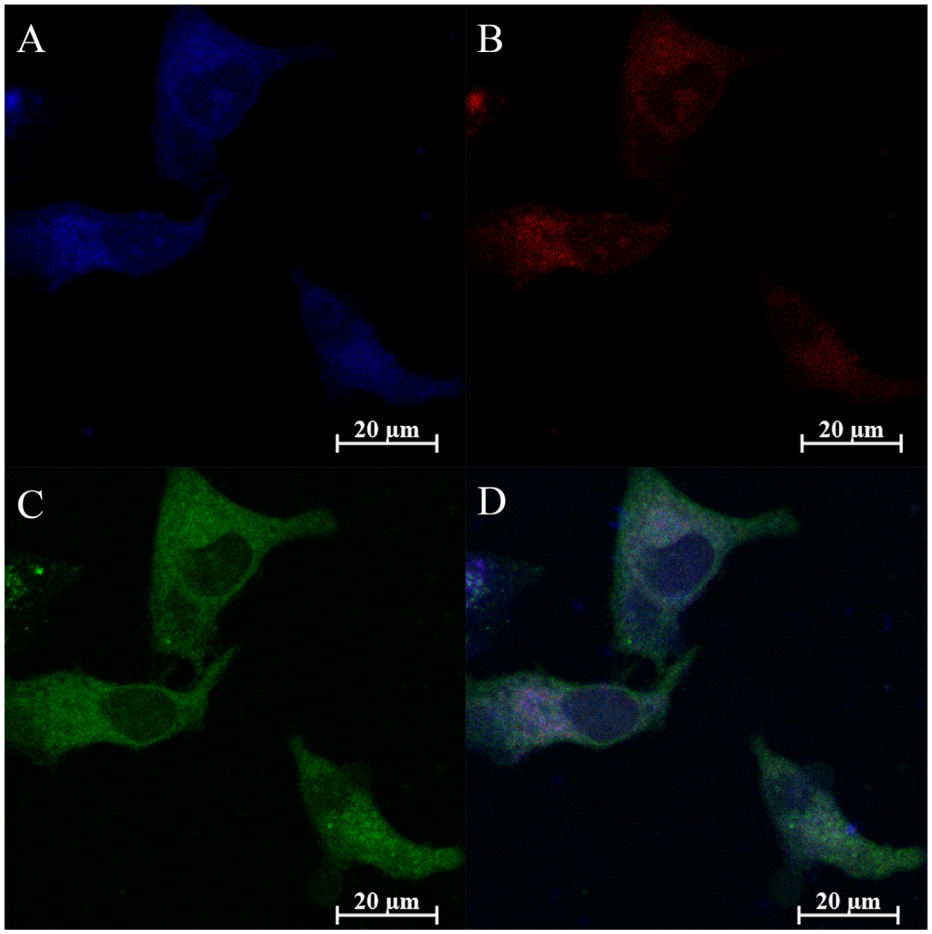

Fig. 4. Confocal fluorescence images of A549 cells. (A-B) Cells treated with MoS2@AuNCs (blue and red channels). (C) Cells treated with LysoTracker Green (green channel). (D) Merged image of (A)–(C). Concentrations: MoS_2@AuNCs, 1 mg mL^{-1}.

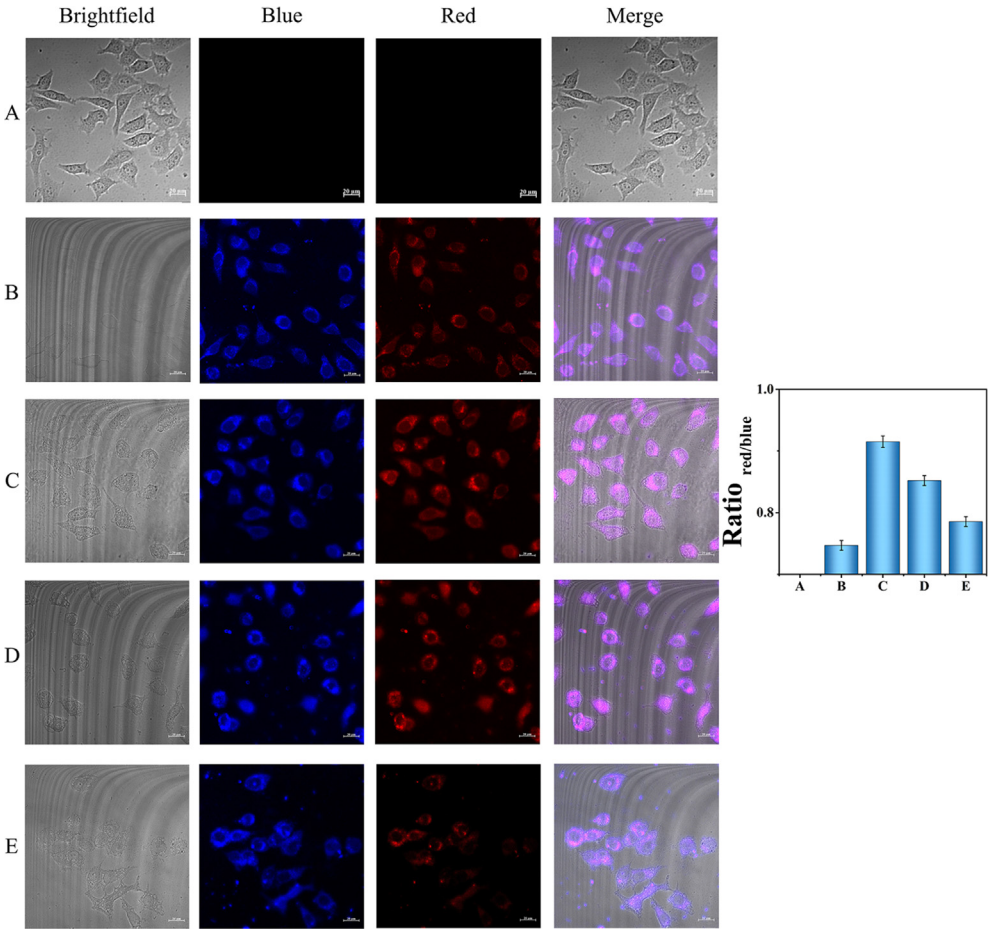

Fig. 5. Confocal fluorescence images of A549 cells. (A) Cells only. (B) Cells incubated with MoS_2@AuNCs for 4 h. (C) Cells incubated with MoS_2@AuNCs for 4 h, followed by Ce^{3+} for 5 min. (D-E) Cells incubated with MoS_2@AuNCs for 4 h, followed by Ce^{3+} and AMP for 15 min (D) and 40 min (E). Concentrations: MoS_2@AuNCs, 1 mg mL^{-1}; Ce^{3+}, 1 mM; and AMP, 20 mM. (F) Fluorescence intensity ratio (F_{red}/F_{blue}) of images in (A)–(E).

were 99.7%-102.5% with the relative standard deviation of 0.4%-2.7%. Furthermore, we measured ALP levels in the above human serum samples using commercial ALP ELISA kits, and the results were consistent with the results obtained by our method, demonstrating that our sensor had satisfactory accuracy.

3.6. Bioimaging of ALP in living cells

The cytotoxicity of the ratiometric sensor was evaluated by MTT assay. As shown in Fig. 3, the viability of A549 cells incubated with MoS_2@AuNCs (with concentrations of up to 1 mg mL^{-1}) for 24 h was nearly 100%, indicating that MoS_2@AuNCs had low toxicity, thus is suitable for bioimaging of living cells.

Encouraged by its excellent biocompatibility, MoS_2@AuNCs was further used in lysosome localization and imaging of intracellular ALP. The subcellular distribution of MoS_2@AuNCs was assessed by co-localization experiments. As shown in Fig. 4, A549 cells treated with MoS_2@AuNCs and LysoTracker Green (a commercial lysosome-specific fluorescent dye) exhibited blue and red fluorescence of MoS_2@AuNCs and green fluorescence of LysoTracker Green. The clear overlap of the above channels indicated that MoS_2@AuNCs had lysosome-targeting ability.

The ability of the sensor in imaging of intracellular ALP was further assessed. Cells in group A (blank control, cells only) did not exhibit fluorescence (Fig. 5A). Cells incubated with MoS_2@AuNCs for 4 h exhibited bright blue fluorescence (blue channel) of MoS_2 QDs and relatively weak red fluorescence (red channel) of AuNCs (Fig. 5B). Upon the addition of Ce^{3+}, the red fluorescence was enhanced while the blue fluorescence was unchanged, which could be used as a reference (Fig. 5C). After being treated with AMP, the red fluorescence signal gradually decreased both after 15 min and 40 min (Fig. 5D&E). Fig. 5F shows the corresponding fluorescence intensity ratio (F_{red}/F_{blue}) in Fig. 5A–E. The above results demonstrate that the developed ratiometric sensor can be applied in imaging of endogenous ALP in living cells, thus may have a great potential in clinical diagnostic applications.

4. Conclusion

To sum up, a ratiometric fluorescent sensor based on MoS_2@AuNCs for ALP detection was developed. The binding between Ce^{3+} and the carboxyl groups of AuNCs could induce AIEE, causing the fluorescence of AuNCs to increase. Meanwhile, the fluorescence of MoS_2 QDs remained constant, thus could be used as a reference signal. Owing to the high affinity between Ce^{3+} and PO_4^{3-} produced from the hydrolysis of AMP by ALP, the fluorescence of AuNCs decreased with increasing concentration of ALP. The sensor had a linear response with ALP concentration ranging from 0.5 to 50 U L^{-1} with an LOD of 0.08 U L^{-1}. With its simplicity, as well as its high selectivity and sensitivity towards ALP, the sensor was successfully further applied in biological imaging of intracellular ALP and lysosome localization, showing that it may have a great potential in clinical diagnosis and other related medical applications.

CRediT authorship contribution statement

Yibing Liu: Methodology, Writing - original draft, Data curation, Investigation. **Yu Zhang:** Writing - original draft, Formal analysis. **Wei Zhang:** Writing - original draft, Investigation. **Xinghua Wang:** Methodology, Project administration, Writing - review & editing. **Ying Sun:** Project administration, Writing - review & editing. **Yibing Huang:** Project administration, Writing - review & editing. **Pinyi Ma:** Project administration, Writing - review & editing. **Jun Ding:** Project administration, Writing - review & editing. **Daqian Song:** Project administration, Writing - review & editing.

Declaration of Competing Interest

The authors declare that they have no known competing financial interests or personal relationships that could have appeared to influence the work reported in this paper.

Acknowledgements

This work was supported by the National Natural Science Foundation of China (Grant nos. 22004046 and 22074052), Science and Technology Developing Foundation of Jilin Province (Grant No. 20200602047ZP).

Appendix A. Supplementary material

Supplementary data to this article can be found online at https://doi.org/10.1016/j.saa.2021.120087.

References

[1] Y. Liu, K.S. Schanze, Conjugated polyelectrolyte-based real-time fluorescence assay for alkaline phosphatase with pyrophosphate as substrate, Anal. Chem. 80 (2008) 8605–8612.
[2] A. Alonso, J. Sasin, N. Bottini, I. Friedberg, I. Friedberg, A. Osterman, A. Godzik, T. Hunter, J. Dixon, T. Mustelin, Protein tyrosine phosphatases in the human genome, Cell 117 (2004) 699–711.
[3] P.Y. Kwo, S.M. Cohen, J.K. Lim, ACG Clinical Guideline: Evaluation of Abnormal Liver Chemistries, American J. Gastroenterol. 112 (2017) 18–35.
[4] U. Sharma, D. Pal, R. Prasad, Alkaline phosphatase: an overview, Indian J. Clin. Biochem. IJCB 29 (2014) 269–278.
[5] M.I. Lassenius, C.L. Fogarty, M. Blaut, K. Haimila, L. Riittinen, A. Paju, J. Kirveskari, J. Jarvela, A.J. Ahola, D. Gordin, M.A. Harma, A. Kumar, S.R. Hamarneh, R.A. Hodin, T. Sorsa, T. Tervahartiala, S. Horkko, P.J. Pussinen, C. Forsblom, M. Jauhiainen, M.R. Taskinen, P.H. Groop, M. Lehto, G. FinnDiane Study, Intestinal alkaline phosphatase at the crossroad of intestinal health and disease - a putative role in type 1 diabetes, Journal of internal medicine, 281 (2017) 586-600.
[6] P. Cohen, The regulation of protein function by multisite phosphorylation – a 25 year update, Trends Biochem. Sci. 25 (2000) 596–601.
[7] L.N. Johnson, R.J. Lewis, Structural basis for control by phosphorylation, Chem. Rev. 101 (2001) 2209–2242.
[8] H. Wang, Y. Li, Y. Zuo, J. Li, S. Ma, L. Cheng, Biocompatibility and osteogenesis of biomimetic nano-hydroxyapatite/polyamide composite scaffolds for bone tissue engineering, Biomaterials 28 (2007) 3338–3348.
[9] R. Williams, R. Aspinall, M. Bellis, G. Camps-Walsh, M. Cramp, A. Dhawan, J. Ferguson, D. Forton, G. Foster, S.I. Gilmore, M. Hickman, M. Hudson, D. Kelly, A. Langford, M. Lombard, L. Longworth, N. Martin, K. Moriarty, P. Newsome, J. O'Grady, R. Pryke, H. Rutter, S. Ryder, N. Sheron, T. Smith, Addressing liver disease in the UK: a blueprint for attaining excellence in health care and reducing premature mortality from lifestyle issues of excess consumption of alcohol, obesity, and viral hepatitis, Lancet 384 (2014) 1953–1997.
[10] X. Gu, G. Zhang, Z. Wang, W. Liu, L. Xiao, D. Zhang, A new fluorometric turn-on assay for alkaline phosphatase and inhibitor screening based on aggregation and deaggregation of tetraphenylethylene molecules, Analyst 138 (2013) 2427–2431.
[11] B.A. Jardin, Y. Zhao, M. Selvaraj, J. Montes, R. Tran, S. Prakash, C.B. Elias, Expression of SEAP (secreted alkaline phosphatase) by baculovirus mediated transduction of HEK 293 cells in a hollow fiber bioreactor system, J. Biotechnol. 135 (2008) 272–280.
[12] T. Arai, T. Nishijo, Y. Matsumae, Y. Zhou, K. Ino, H. Shiku, T. Matsue, Noninvasive measurement of alkaline phosphatase activity in embryoid bodies and coculture spheroids with scanning electrochemical microscopy, Anal. Chem. 85 (2013) 9647–9654.
[13] X. Chen, J. Chen, H.-Y. Zhang, F.-B. Wang, F.-F. Wang, X.-H. Ji, Z.-K. He, Colorimetric Detection of Alkaline Phosphatase on Microfluidic Paper-based Analysis Devices, Chin. J. Anal. Chem. 44 (2016) 591–596.
[14] H. Jiao, J. Chen, W. Li, F. Wang, H. Zhou, Y. Li, C. Yu, Nucleic acid-regulated perylene probe-induced gold nanoparticle aggregation: a new strategy for colorimetric sensing of alkaline phosphatase activity and inhibitor screening, ACS Appl. Mater. Interf. 6 (2014) 1979–1985.
[15] Y. Liu, E. Xiong, X. Li, J. Li, X. Zhang, J. Chen, Sensitive electrochemical assay of alkaline phosphatase activity based on TdT-mediated hemin/G-quadruplex DNAzyme nanowires for signal amplification, Biosens. Bioelectron. 87 (2017) 970–975.
[16] C. Shen, X. Li, A. Rasooly, L. Guo, K. Zhang, M. Yang, A single electrochemical biosensor for detecting the activity and inhibition of both protein kinase and alkaline phosphatase based on phosphate ions induced deposition of redox precipitates, Biosens. Bioelectron. 85 (2016) 220–225.
[17] J. Zhang, L. He, X. Zhang, J. Wang, L. Yang, B. Liu, C. Jiang, Z. Zhang, Colorimetric and SERS dual-readout for assaying alkaline phosphatase activity by ascorbic acid induced aggregation of Ag coated Au nanoparticles, Sens. Actuat. B 253 (2017) 839–845.
[18] C. Ruan, W. Wang, B. Gu, Detection of alkaline phosphatase using surface-enhanced Raman spectroscopy, Anal. Chem. 78 (2006) 3379–3384.
[19] Z. Qian, L. Chai, Q. Zhou, Y. Huang, C. Tang, J. Chen, H. Feng, Reversible Fluorescent Nanoswitch Based on Carbon Quantum Dots Nanoassembly for Real-Time Acid Phosphatase Activity Monitoring, Anal. Chem. 87 (2015) 7332–7339.
[20] F. Wang, C. Zhang, Q. Xue, H. Li, Y. Xian, Label-free upconversion nanoparticles-based fluorescent probes for sequential sensing of Cu(2+), pyrophosphate and alkaline phosphatase activity, Biosens. Bioelectron. 95 (2017) 21–26.
[21] N. Li, Y. Li, Y. Han, W. Pan, T. Zhang, B. Tang, A highly selective and instantaneous nanoprobe for detection and imaging of ascorbic acid in living cells and in vivo, Anal. Chem. 86 (2014) 3924–3930.
[22] K. Zhang, H. Zhou, Q. Mei, S. Wang, G. Guan, R. Liu, J. Zhang, Z. Zhang, Instant visual detection of trinitrotoluene particulates on various surfaces by ratiometric fluorescence of dual-emission quantum dots hybrid, J. Am. Chem. Soc. 133 (2011) 8424–8427.
[23] H. Mishra, S.K. Singh, V.K. Singh, J. Singh, S. Srikrishna, A. Srivastava, Highly stable and bio-compatible luminescent molybdenum disulfide quantum dots for imaging of alimentary canal in Drosophila, J. Lumin. 202 (2018) 111–117.
[24] H. Dong, S. Tang, Y. Hao, H. Yu, W. Dai, G. Zhao, Y. Cao, H. Lu, X. Zhang, H. Ju, Fluorescent MoS_2 Quantum Dots: Ultrasonic Preparation Up-Conversion and Down-Conversion Bioimaging, and Photodynamic Therapy, ACS Appl. Mater. Interf. 8 (2016) 3107–3114.
[25] X. Wang, Y. Wang, H. He, X. Ma, Q. Chen, S. Zhang, B. Ge, S. Wang, W.M. Nau, F. Huang, Deep-Red Fluorescent Gold Nanoclusters for Nucleoli Staining: Real-Time Monitoring of the Nucleolar Dynamics in Reverse Transformation of Malignant Cells, ACS Appl. Mater. Interf. 9 (2017) 17799–17806.
[26] T. Shu, L. Su, J. Wang, X. Lu, F. Liang, C. Li, X. Zhang, Value of the Debris of Reduction Sculpture: Thiol Etching of Au Nanoclusters for Preparing Water-Soluble and Aggregation-Induced Emission-Active Au(I) Complexes as Phosphorescent Copper Ion Sensor, Anal. Chem. 88 (2016) 6071–6077.
[27] Y.Q. Wang, T. Zhao, X.W. He, W.Y. Li, Y.K. Zhang, A novel core-satellite CdTe/Silica/Au NCs hybrid sphere as dual-emission ratiometric fluorescent probe for Cu^{2+}, Biosens. Bioelectron. 51 (2014) 40–46.
[28] J.G. You, C.Y. Lu, A.S. Krishna Kumar, W.L. Tseng, Cerium(iii)-directed assembly of glutathione-capped gold nanoclusters for sensing and imaging of alkaline phosphatase-mediated hydrolysis of adenosine triphosphate, Nanoscale 10 (2018) 17691–17698.
[29] L.J. Sun, L. Qu, R. Yang, L. Yin, H.J. Zeng, Cysteamine functionalized MoS_2 quantum dots inhibit amyloid aggregation, Int. J. Biol. Macromol. 128 (2019) 870–876.
[30] H. Wang, L. Da, L. Yang, S. Chu, F. Yang, S. Yu, C. Jiang, Colorimetric fluorescent paper strip with smartphone platform for quantitative detection of cadmium ions in real samples, J. Hazard. Mater. 392 (2020) 122506.
[31] L. Lai, L. Chen, D. Zhan, L. Sun, J. Liu, S.H. Lim, C.K. Poh, Z. Shen, J. Lin, One-step synthesis of NH_2-graphene from in situ graphene-oxide reduction and its improved electrochemical properties, Carbon 49 (2011) 3250–3257.
[32] F. Mo, Z. Ma, T. Wu, M. Liu, Y. Zhang, H. Li, S. Yao, Holey reduced graphene oxide inducing sensitivity enhanced detection nanoplatform for cadmium ions based on glutathione-gold nanocluster, Sens. Actuat. B 281 (2019) 486–492.
[33] F. Ru, P. Du, X. Lu, Efficient ratiometric fluorescence probe utilizing silicon particles/gold nanoclusters nanohybrid for "on-off-on" bifunctional detection and cellular imaging of mercury (II) ions and cysteine, Anal. Chim. Acta 1105 (2020) 139–146.
[34] H. Yu, Y. Liu, J. Wang, Q. Liang, H. Liu, J. Xu, S. Shao, A gold nanocluster-based ratiometric fluorescent probe for cysteine and homocysteine detection in living cells, New J. Chem. 41 (2017) 4416–4423.
[35] H. Liu, L. Jia, Y. Wang, M. Wang, Z. Gao, X. Ren, Ratiometric fluorescent sensor for visual determination of copper ions and alkaline phosphatase based on carbon quantum dots and gold nanoclusters, Anal. Bioanal. Chem. 411 (2019) 2531–2543.
[36] S. Liu, F. Shi, X. Zhao, L. Chen, X. Su, 3-Aminophenyl boronic acid-functionalized $CuInS_2$ quantum dots as a near-infrared fluorescence probe for the determination of dopamine, Biosens. Bioelectron. 47 (2013) 379–384.
[37] X. Liu, H. Yuan, D. Pang, R. Cai, Resonance light scattering spectroscopy study of interaction between gold colloid and thiamazole and its analytical

application, Spectrochim. Acta Part A Mol. Biomol. Spectrosc. 60 (2004) 385–389.
[38] D. Li, J. Qin, Q. Xu, G. Yan, A room-temperature phosphorescence sensor for the detection of alkaline phosphatase activity based on Mn-doped ZnS quantum dots, Sens. Actuat. B 274 (2018) 78–84.
[39] Z. Qian, L. Chai, C. Tang, Y. Huang, J. Chen, H. Feng, Carbon quantum dots-based recyclable real-time fluorescence assay for alkaline phosphatase with adenosine triphosphate as substrate, Anal. Chem. 87 (2015) 2966–2973.